Coupling non-thermal plasma with Ni catalysts supported on BETA zeolite for catalytic CO_2 methanation

Supporting Information (SI)

1. Performance of non-thermal plasma (NTP)-assisted CO_2 methanation over BETA zeolites and La/Na-BETA catalyst

The catalytic CO_2 methanation performance has been tested over the La/Na-BETA catalyst with 20 wt.% La loading under the NTP condition, and the results are shown in Fig. S1. This catalyst was found to be inactive under NTP conditions, showing a very low CO_2 conversion of *ca.* 10%, which could be related to the gas phase reaction induced by NTP.
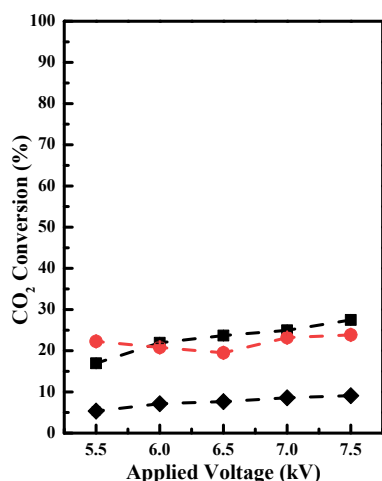

Fig. S1. Catalytic performances of H-BETA, Na-BETA zeolites and 20wt.%La/Na-BETA catalyst in NTP-activated CO hydrogenation: (a) CO_2 conversion, (b) CH_4 selectivity, and (c) CO selectivity (feed gas composition of $H_2/CO_2 = 4$, WHSV of 23,077 ml (STP) $g_{cat}^{-1} h^{-1}$).

In terms of the catalytic CO_2 methanation performance over the developed catalysts (*e.g.* 15Ni/H-BETA, 15Ni/Na-BETA) under NTP conditions (shown in Fig. 2), at low applied voltage of 6.0 kV, we realised that the value of sum of CH_4 and CO selectivity is lower than the 100%. Accordingly, the carbon balance was calculated based only on the gaseous products (*i.e.* CO, CH_4, and CO_2) from the exit of reactor, showing that there was *ca.* 15% carbon loss. There are three possible reasons for accounting for the measured carbon loss of the reaction: (1) the measurement errors including gas chromatography (GC) measurements, measurements of gas flow rate *via* a bubble flow meter, *etc*; (2) the carbon species adsorbed on the catalyst surface under low temperature plasma conditions, which can be clearly observed in the Figs. 7–9; (3) the formation of liquid products (*e.g.* methanol and formic acid) in the catalytic system.

During the NTP catalytic CO_2 methanation experiments, only the gaseous products (*i.e.* CO, CH_4, and CO_2) were measured and quantified using the in-line GC. For the liquid products, they were condensed using an ice bath, however were not quantified since they are accumulated in the condenser (it was difficult to correlate the data as a function of time-on-stream). In order to examine the liquid products,

we analysed the mass spectrometry (MS) signals collected from the exit of the DRIFTS cell when we performed the *in situ* DRIFTS experiments. Figs. S2–S4 shows the MS signals collected at the exit of the DRIFTS cell loaded with different catalysts (*i.e.* 15Ni/H-BETA, 15Ni/Na-BETA, and 15Ni-20La/Na-BETA catalyst), respectively. Clearly, with the ignition of NTP, the MS profiles for all the catalysts show the emerging of the lines at m/z = 29 and 31, confirming the production of methanol and formic acid during the catalysis. Since the work concerns the production of gaseous CH_4 *via* the catalytic CO_2 hydrogenation, the detailed analysis of the selectivity and yield of the liquid products (*e.g.* methanol and formic acid) are not determined.
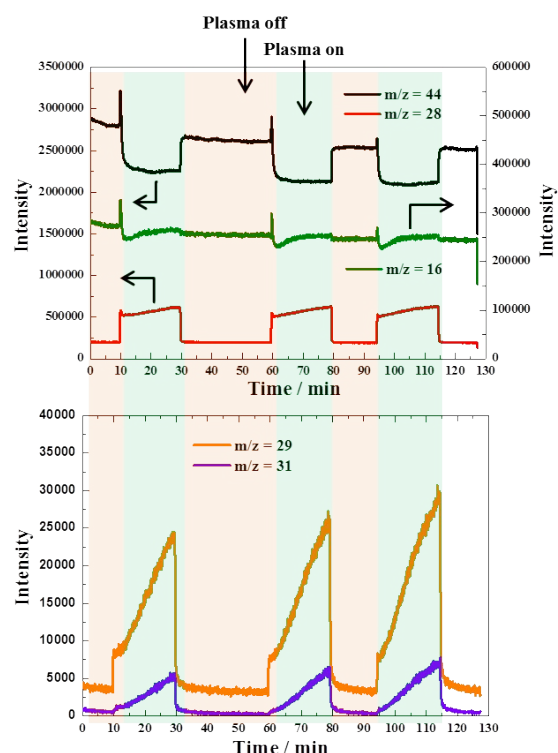

Fig. S2. MS signals collected at the exit of the DRIFTS cell loaded with 15Ni/H-BETA catalyst as a function of time during the NTP-assisted catalytic CO_2 methanation at ambient temperature (feed gas composition: 4% CO_2/16% H_2 diluted in Argon, applied peak voltage = 6.0 kV, frequency = 26 kHz).
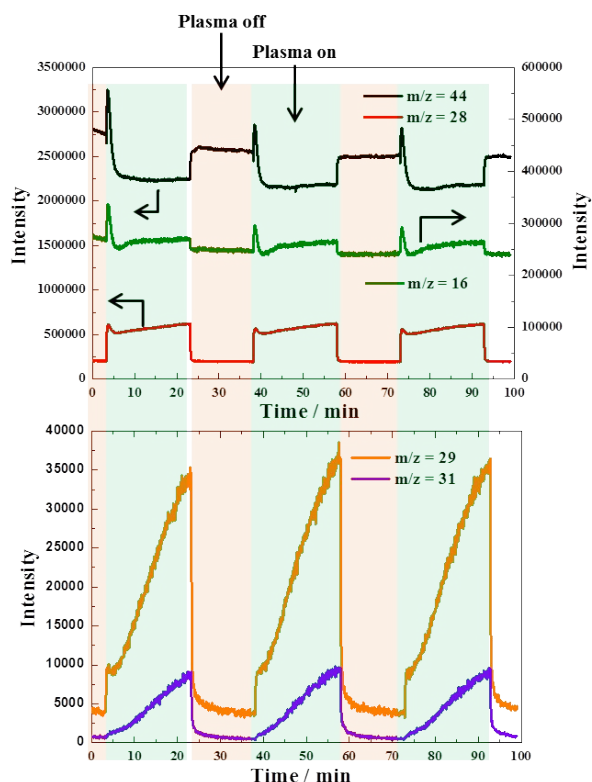
2

Fig. S3. MS signals collected at the exit of the DRIFTS cell loaded with 15Ni/Na-BETA catalyst as a function of time during the NTP-assisted catalytic CO_2 methanation at ambient temperature (feed gas composition: 4% CO_2/16% H_2 diluted in Argon, applied peak voltage = 6.0 kV, frequency = 26 kHz).
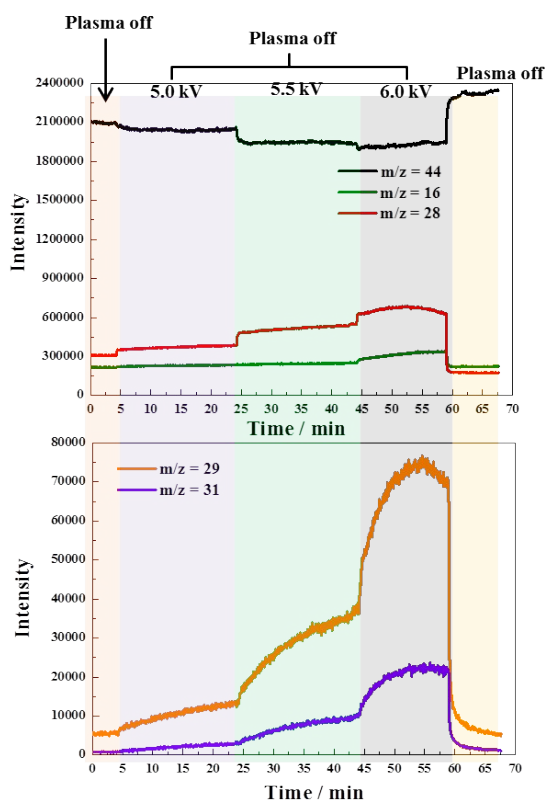

Fig. S4. MS signals collected at the exit of the DRIFTS cell loaded with 15Ni-20La/Na-BETA catalyst as a function of time during the NTP-assisted catalytic CO_2 methanation at ambient temperature (feed gas composition: 4% CO_2/16% H_2 diluted in Argon, applied peak voltage = 5.0-6.0 kV, frequency = 26 kHz).

3

2. Calculation of the equilibrium conversion

The calculation for the equilibrium conversions as a function of the reaction temperature ($H_2/CO_2 = 4$, $P = 1$ bar) was implemented with the aid of Aspen Plus 8.0. In Aspen Plus, RGibbs (Rigorous reaction and/or multiphase equilibrium based on Gibbs free energy minimisation) was selected as a model to perform the simulation, and on top of that, the sensibility analysis was applied as a model analysis tool to investigate the impact of temperature.

3. Characterisation of the catalysts

The determination of actual metal amounts in prepared catalysts was carried out by using a Quant PQ 900 inductively coupled plasma optical emission spectrometer (ICP-OES). Prior to test, the samples (~25 mg) were mixed with 12 ml aqua regia and digested in an ETHOS UP microwave digester for 20 mins under 220 ºC.

Table S1. Inductively Coupled Plasma Optical Emission Spectroscopy (ICP-OES) analysis of the as-synthesised catalysts.

Sample	Ni (wt.%)	La (wt.%)	Na (wt.%)
15Ni/H-BETA	13.97±0.23	-	-
15Ni/Na-BETA	14.84±0.49	-	3.14±0.09
15Ni-5La/Na-BETA	12.88±0.11	4.85±0.09	5.48±0.05
15Ni-10La/Na-BETA	12.51±0.12	9.25±0.11	5.83±0.13
15Ni-20La/Na-BETA	11.04±0.37	15.51±0.52	5.57±0.10

H_2 pulse chemisorption was performed over Micromeritics AutoChem II 2920 instrument to measure the nickel dispersion and active nickel surface areas. The samples were reduced at 673 K for 1 h under 10% H_2/Ar flow (30 mL/min) and then were cooled down to 323 K. The H_2 pulse chemisorption was then carried out by pulsing of a mixture of 10% H_2/Ar (30 mL/min). The results are listed in Table S2.

Table S2. H_2 pulse chemisorption results.

Sample	Ni dispersion (%)	Active Ni surface areas ($m^2 g_{Ni}^{-1}$)
15Ni/H-BETA	3.82	25.41
15Ni/Na-BETA	1.80	11.99
15Ni-5La/Na-BETA	1.65	10.99
15Ni-10La/Na-BETA	1.53	10.16
15Ni-20La/Na-BETA	1.75	11.66

Fig. S5 reports the N_2 physisorption isotherms of different catalysts developed in this work, and their corresponding textural and structural properties are also presented in Table S3. Fig. S5 shows that both

H-BETA and Na-BETA zeolites give similar N_2 physisorption type IV isotherms, presenting typical hysteresis loop at relative pressures (P/P^0) between 0.5 and 1. This result indicates the existence of mesoporous structures in BETA zeolite which are beneficial to the impregnation of high metal loading [1]. However, the size of the hysteresis loop decreases regardless of the exchange of Na^+ and the impregnation of Ni^+ in BETA zeolite. In addition, significant decreases in specific surface area, micropore and mesopore volumes are observed in this work, as shown in Table S3, confirming that the introduction of Na^+, the formation of NiO and La_2O_3 clusters could block the micropores in BETA zeolite and, accordingly, reduce the adsorption capacity [2, 3].
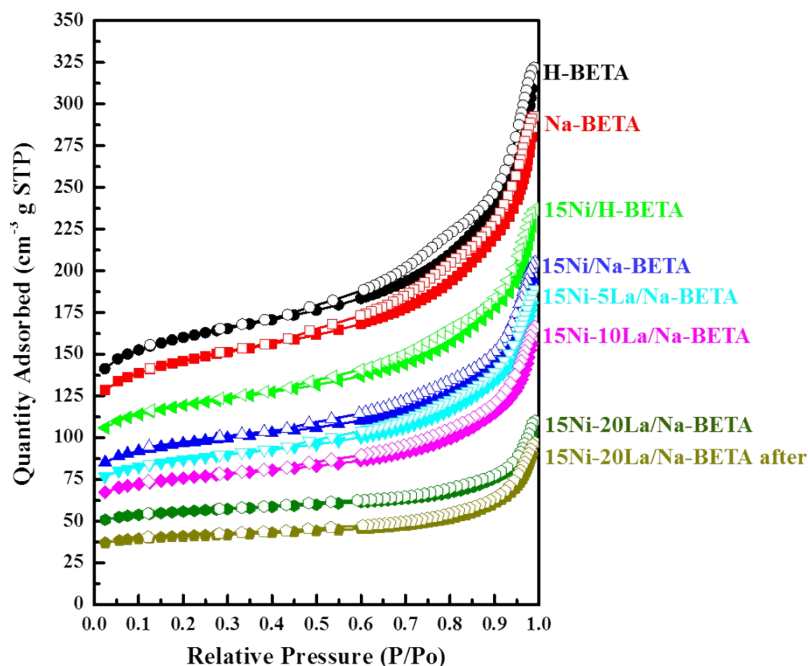

Fig. S5. N_2 physisorption isotherms of different samples.

Table S3. Textural and structural properties of different samples.

Sample	S_{BET} (m^2 g^{-1})^a	V_{micro} (cm^3 g^{-1})^b	V_{meso} (cm^3 g^{-1})^b
H-BETA	500	0.18	0.30
Na-BETA	457	0.16	0.27
15Ni/H-BETA	373	0.14	0.21
15Ni/Na-BETA	301	0.11	0.19
15Ni-5La/Na-BETA	271	0.10	0.18
15Ni-10La/Na-BETA	236	0.09	0.16
15Ni-20La/Na-BETA	172	0.07	0.09
15Ni-20La/Na-BETA after ^{c}	127	0.05	0.09

^{a} Calculated by complete BET equation; ^{b} Determined by application of BJH method; ^{c} Refer to the 15Ni-20La/Na-BETA catalysts after tested in NTP assisted CO_2 methanation.

The morphology of the catalysts was also examined using the transmission electron microscopy (TEM). TEM images of 15Ni-20La/Na-BETA catalysts measured before and after NTP-assisted CO_2 methanation are presented in Fig. S6, respectively. The black spots could be the mixed Ni-La metal

species, which are well dispersed over Na-BETA zeolite support before and after NTP-activated CO_2 methanation. However, the Ni-La species exhibit aggregation to some extent. Therefore, it is difficult to determine the average metal particles in prepared catalysts accurately.
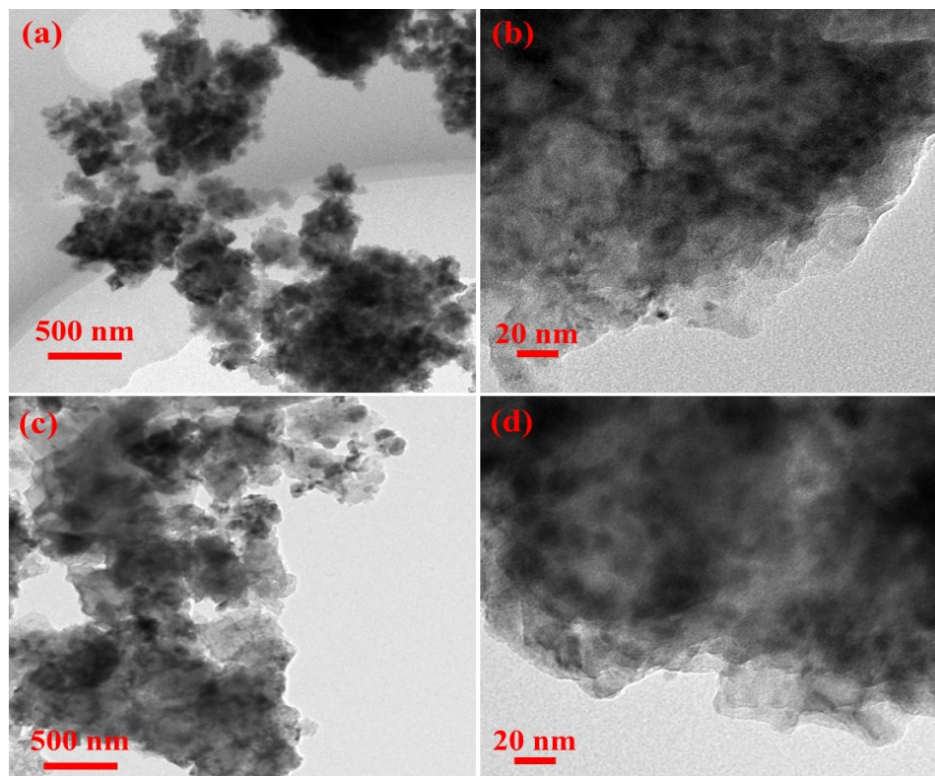

Fig. S6. TEM micrographs of 15Ni-20La/Na-BETA catalysts before (a and b) and after (c and d) NTP-assisted catalytic CO_2 methanation.

Fig. S7 shows XRD patterns of the protonic zeolite (H-BETA) and sodium exchanged zeolite (Na-BETA), and the corresponding catalysts. It can be observed in Fig. S7a and b that the diffractogram of Na-BETA zeolite is almost identical to that of H-BETA, indicating the incorporation of Na^+ only affect the zeolite crystalline nature slightly. In addition, the characteristic peak of Na_2O cannot be observed in the XRD spectra, confirming the successful exchange of Na^+ in the zeolite framework [1]. XRD spectra also show three diffraction peaks at $2\theta = 37, 43$ and $63°$ (marked with dots), which could be attributed to the bunsenite phase of NiO [4]. Interestingly, regarding the catalysts post NTP-assisted catalytic CO_2 methanation, the XRD spectra present the new diffraction peaks at $2\theta = 44$ and $52°$ (marked with squares), indicating the formation of elemental Ni in the catalysts [5]. This result confirms that NiO species in catalysts were reduced during the NTP-assisted catalytic CO_2 methanation. XRD spectra of Na-BETA supported Ni catalysts after the impregnation of different amounts of La are presented in Fig. S7c. After the introduction of La, XRD spectra of the fresh catalysts show similar diffraction peaks at $2\theta = 37, 43$ and $63°$ which corresponds to NiO, whereas that of tested catalysts show peaks at $2\theta = 44$ and $52°$ which are characteristic of elemental Ni.
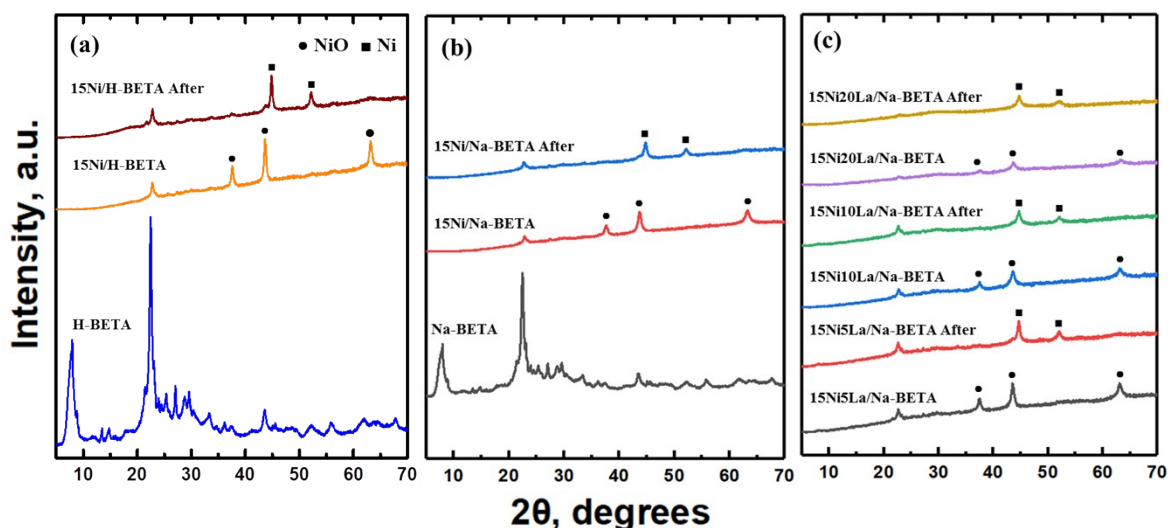
Fig. S7 XRD patterns of (a) the H-BETA zeolite supported Ni catalysts, (b) the Na-BETA zeolite supported Ni catalysts, and (c) the Ni-La/Na-BETA catalysts with different nominal content of La.

The developed zeolite catalysts were examined by H_2-TPR technique in order to determine their redox properties and reduction behaviours. Specifically, Figs. S8b and S8e show the hydrogen consumption profiles of the 15Ni/Na-BETA and 15Ni-20La/Na-BETA catalysts, respectively. The reduction profile of the as-prepared 15Ni/Na-BETA catalyst exhibits a broad reduction peak located between 400 and 700 °C which consists of two main peaks, *i.e.* about 500 and 650 °C. The first peak is attributed to the reduction of NiO species located on the external surface of Na-BETA zeolite [3, 6, 7], while the second peak is related to Ni^{2+} located inside BEA framework [1, 8-11]. Similar reduction behaviour is also observed in terms of the as-prepared 15Ni/H-BETA catalyst (as shown in Fig. S8a). Nevertheless, the H_2-TPR profile of as-synthesised 15Ni-20La/Na-BETA catalyst shows a main H_2 consumption peak located at *ca.* 450 °C, which is attributed to the reduction of NiO species located on the external surface of the zeolite [12, 13]. It should be noted that the reducibility of catalysts was improved slightly after the addition of La. As listed in Table S4, the total H_2 consumption (mmol g^{-1} of catalyst) increased from 2.89 (15Ni/Na-BETA) to 3 (15Ni-20La/Na-BETA). Before performing the NTP-assisted CO_2 hydrogenation catalysis, all the as-prepared catalysts were pre-treated in the pure H_2 flow with a flow rate of 50 mL min^{-1} for 30 min under the NTP condition (applied peak voltage: 7 kV, frequency: 20.3 kHz). Therefore, the H_2 reduction behaviour of the 15Ni-20La/Na-BETA catalyst after plasma pre-treatment was measured as well. It can be seen in Fig. S8e that the pre-treated catalyst presents a main H_2 consumption peak located at a relatively low temperature of *ca.* 400 °C in comparison with fresh catalyst. The total H_2 consumption declined to 2.36, indicating that NiO species have been partially reduced to elemental Ni during the H_2 plasma pre-treatment. Interestingly, after NTP-assisted CO_2 methanation, similar reduction behaviour can be observed, confirming that the characteristics of active sites remain stable during the plasma activation. Furthermore, the reduction peak of 15Ni-20La/Na-BETA after H_2 plasma pre-treatment is more intense than that of the used catalyst, and the corresponding H_2 consumption further decreases from 2.36 to 1.62, indicating that the NiO species in catalyst were further reduced to elemental Ni during the NTP-assisted CO_2 hydrogenation process. Similar results can also be observed concerning other catalysts developed by this work (Fig. S8). These results confirm the XRD results shown above.

Furthermore, CO-TPD for the catalysts was measured as well since that the hydrogenation of CO species could be likely the rate determining step [14]. Additionally, the adsorption of CO species and corresponding strength can be examined *via* CO-TPD. As shown in Fig. S9, all the catalysts present

only one main peak located between 200 and 450 °C which can be assigned to the molecularly adsorbed CO [15]. Specifically, the CO desorption temperatures of both 15Ni/Na-BETA and 15Ni-20La/Na-BETA catalysts are higher than that of 15Ni/H-BETA. It must be noted that no CO desorption peak can be observed at the temperature below 75 °C, indicating that $Ni(CO)_4$ species are not formed in all the catalysts, which could accelerate the catalysts deactivation [15].
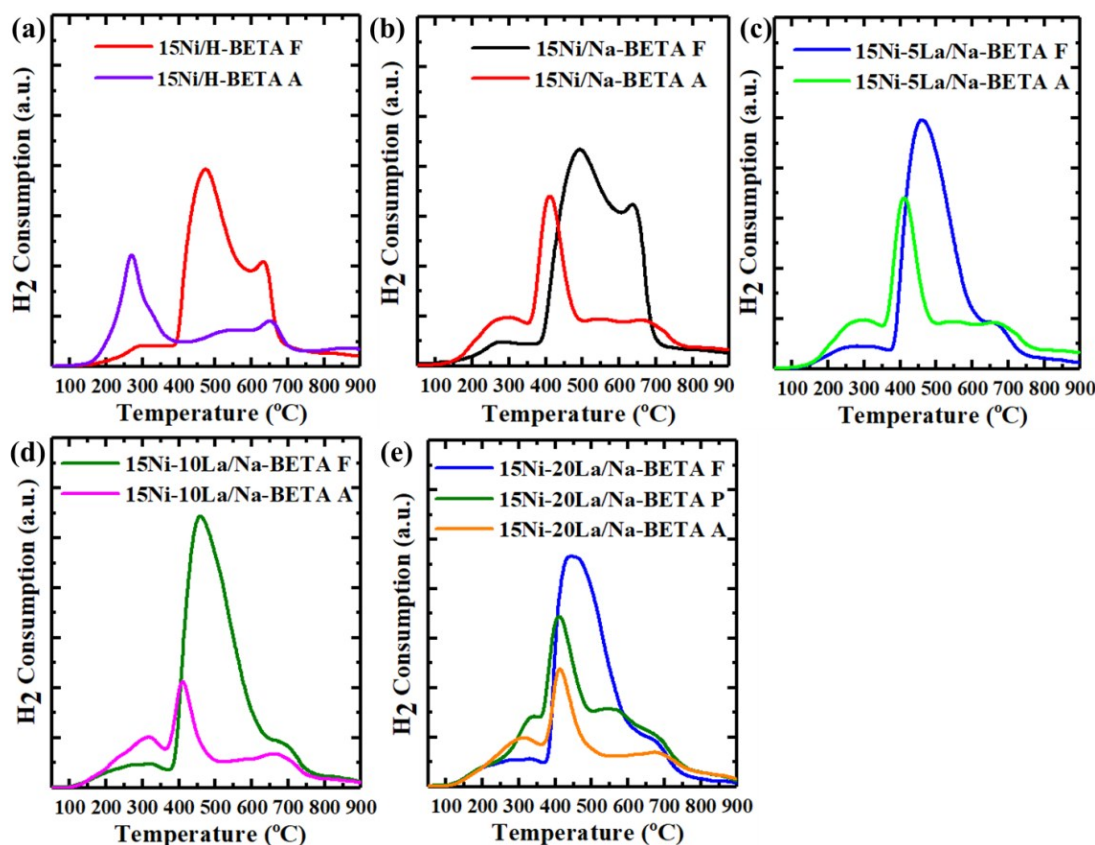

Fig. S8. H_2-TPR profiles for different catalysts (F and A refer to fresh and used catalyst after tested for NTP assisted CO_2 methanation, respectively, whereas P refers to catalyst pre-treated in pure H_2 flow under NTP conditions).

Table S4. Quantitative total H_2 consumption of different catalysts.

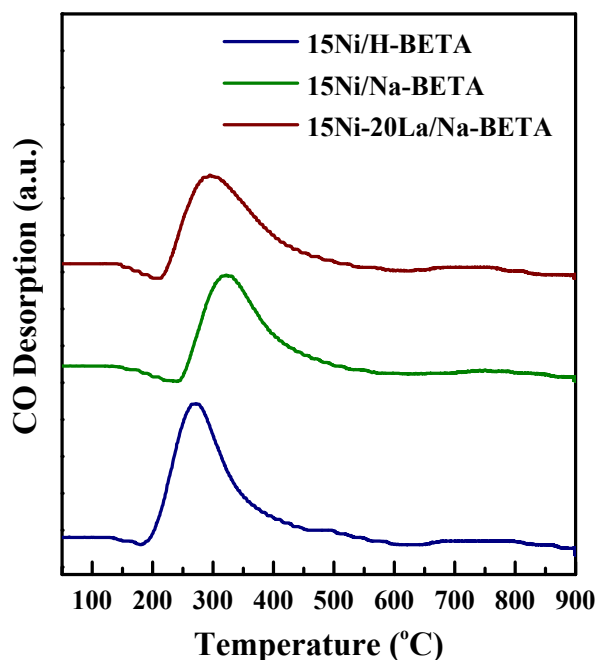| Catalyst	Total H_2 consumption (mmol $g_{catalyst}^{-1}$)
15Ni/Na-BETA fresh	2.89
15Ni/Na-BETA after plasma reaction	1.45
15Ni-20La/Na-BETA fresh	3
15Ni-20La/Na-BETA after H_2 plasma treatment	2.36
15Ni-20La/Na-BETA after plasma reaction	1.62

8

Fig. S9. CO-TPD profiles of different samples.

XPS measurements were also carried out in order to analyse the nature and surface distribution of metal sites. Figs. S10a, d and e show the XPS spectra regarding the Ni 2p, and La 3d core levels for as-synthesised 15Ni/Na-BETA and 15Ni-20La/Na-BETA catalysts, as well as the used catalyst after NTP, assisted catalytic CO_2 hydrogenation. It can be seen in Fig. S10a that the XPS spectrum of 15Ni/Na-BETA catalyst mainly consists of Ni $2p_{1/2}$ and Ni $2p_{3/2}$ regions. Specifically, the Ni $2p_{3/2}$ region shows two peaks at *ca.* 852 and 854 eV as well as a broad shake-up satellite peak at *ca.* 860 eV. Two main peaks at the relatively low binding energy (*i.e.* 852 and 870 eV) are attributed to the octahedral NiO species weakly interacting with Na-BETA zeolite, whereas the peaks at 854 and 872 eV are probably related to the framework pseudo-tetrahedral Ni (II) (*e.g.* Ni-O-Si species) [1, 8]. It must be noted that no peak at *ca.* 853 eV which is related to the reduced nickel (Ni^0) can be detected. After the addition of La in the 15Ni/Na-BETA catalyst, the XPS spectrum of 15Ni-20La/Na-BETA catalyst (Fig. S10d) reveals a new region (*i.e.* La $3d_{5/2}$) which consists of two peaks. The main peak at *ca.* 833 eV could be assigned to the supported La^{3+}, whilst the peak at *ca.* 837 eV is related to the satellite peak [16]. Similar peaks were also identified in Figs. S10b and S10c for the catalysts with different La nominal contents (*i.e.* 5 and 10 wt.%). It should be noted that the intensity of the two peaks increased with the increase in the La content, confirming the loading amount of La in the two catalysts. In addition, in the Ni $2p_{3/2}$ - La $2p_{3/2}$ region (Fig. S10d), the XPS spectrum reveals a new main peak at *ca.* 850 eV and its satellite peak at *ca.* 852 eV, which are all corresponded to the La^{3+} [1]. It can also be observed that the intensity of these two peaks gradually increases as the La contents in catalysts increasing. Additionally, in the XPS spectrum of 15Ni-20La/Na-BETA catalyst, the presence of shake-up satellite peaks for Ni $2p_{1/2}$ and Ni $2p_{3/2}$ at *ca.* 877 and 860 eV confirms that the status of Ni species in the catalyst is in the second oxidation state [17]. Specifically, the main peaks of Ni $2p_{1/2}$ at *ca.* 871 eV and Ni $2p_{3/2}$ at *ca.* 854 eV could be assigned to pseudo-tetrahedral Ni (II), suggesting that Ni active sites are being in strong interaction with the Na-BETA zeolite framework [8]. Furthermore, the XPS spectrum of used 15Ni-20La/Na-BETA catalyst (tested in NTP-assisted catalytic CO_2 hydrogenation) was also examined in order to probe any structural changes of active sites induced by plasma. In comparison with the fresh catalyst, the XPS spectrum shown in Fig. S10e presents similar binding energy region of La^{3+} at La $3d_{5/2}$ region which means that the La_2O_3 species did not change

significantly during the NTP-activated CO_2 hydrogenation. However, it should be noted that the intensity of main peaks in the Ni $2p_{1/2}$ and Ni $2p_{3/2}$ decreases slightly, whereas the intensity of the main peak at *ca.* 850 eV increases significantly, indicating the NiO species were partially reduced into metallic Ni during the plasma-activated reaction. This result is in agreement with the results by XRD and H_2-TPR analysis (as shown in Fig. S7 and 8). This phenomenon is somehow consistent with that of the thermally activated CO_2 methanation mechanisms reported by the literatures. For example, Alcalde-Santiago et al. [18] recently reported that part of the nickel species could be reduced to metallic nickel during thermally catalytic CO_2 methanation.
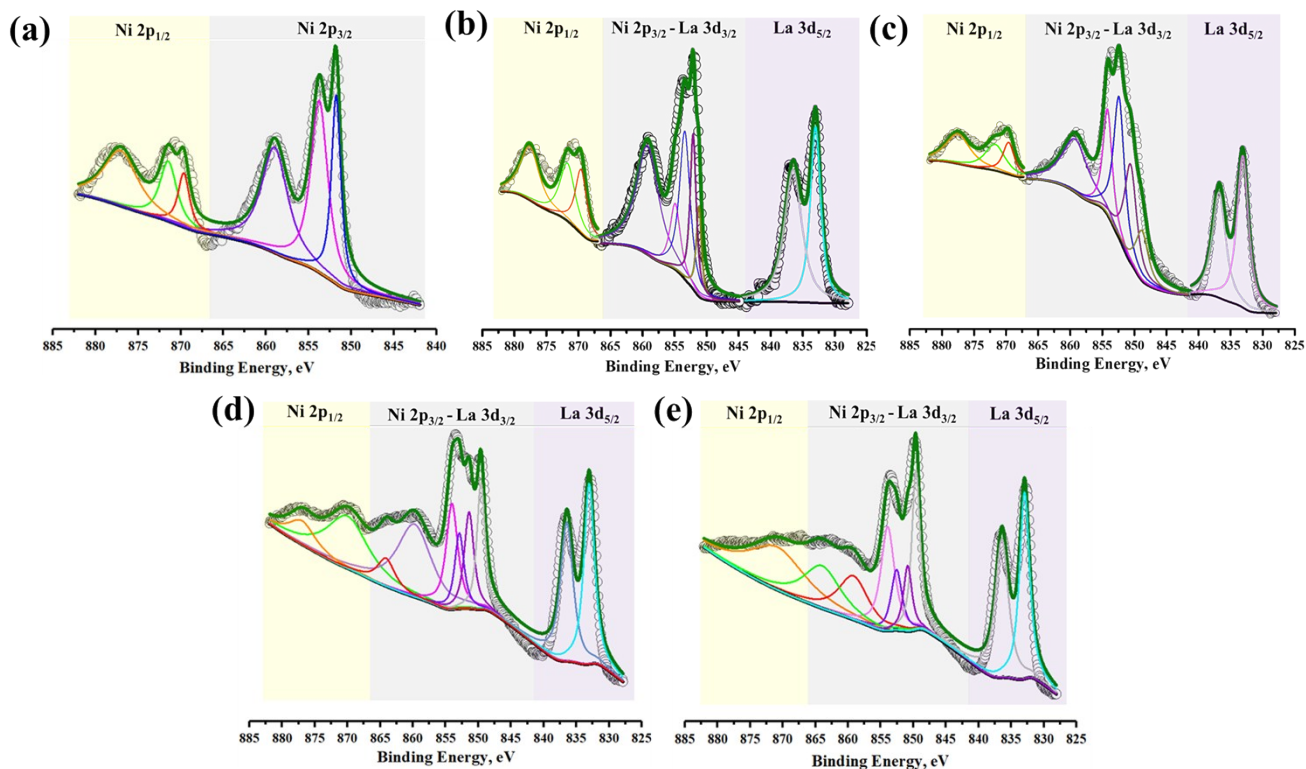

Fig. S10. XPS spectra of different catalysts: (a) 15Ni/Na-BETA, (b) 15Ni-5La/Na-BETA, (c) 15Ni-10La/Na-BETA, (d) fresh and (e) used 15Ni-20La/Na-BETA.

10

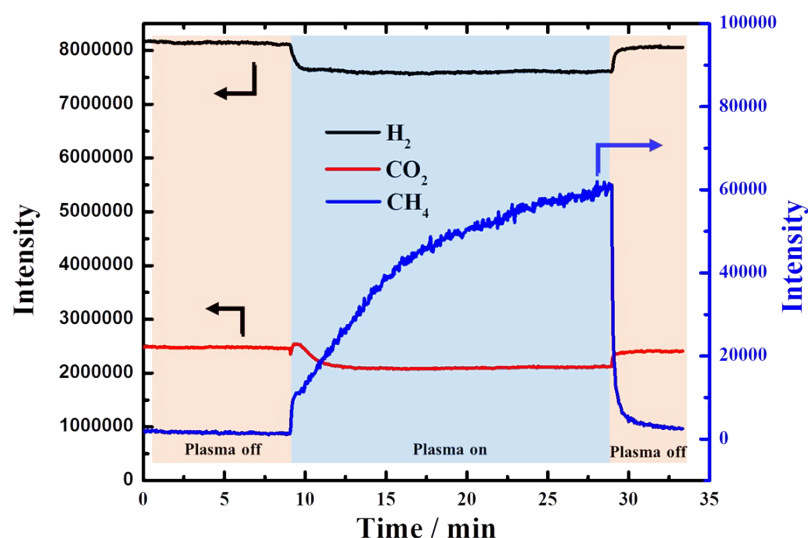# 4. Mechanistic study of NTP-assisted catalytic CO_2 methanation

Fig. S11. MS signals collected at the exit of the DRIFTS cell loaded with 15Ni-20La/Na-BETA catalyst as a function of time during the NTP-assisted catalytic CO_2 methanation at ambient temperature (feed gas composition: 4% CO_2/16% H_2 diluted in Argon, applied peak voltage = 6.0 kV, frequency = 26 kHz).

Comparison of the IR spectra in the wavenumber range (3,500 – 3,800 cm^{-1}) corresponding to zeolite hydroxyl groups is presented in Fig. S12. It can be seen in Fig. S12 that the intensity of IR bands for zeolite hydroxyl groups increased in the presence of La_2O_3. This is consistent with the conclusions reported by Huang et al.[19] In this paper, they concluded that bridging OH groups can be formed on zeolites *via* the Hirschler-Plank mechanism in the presence of La species.
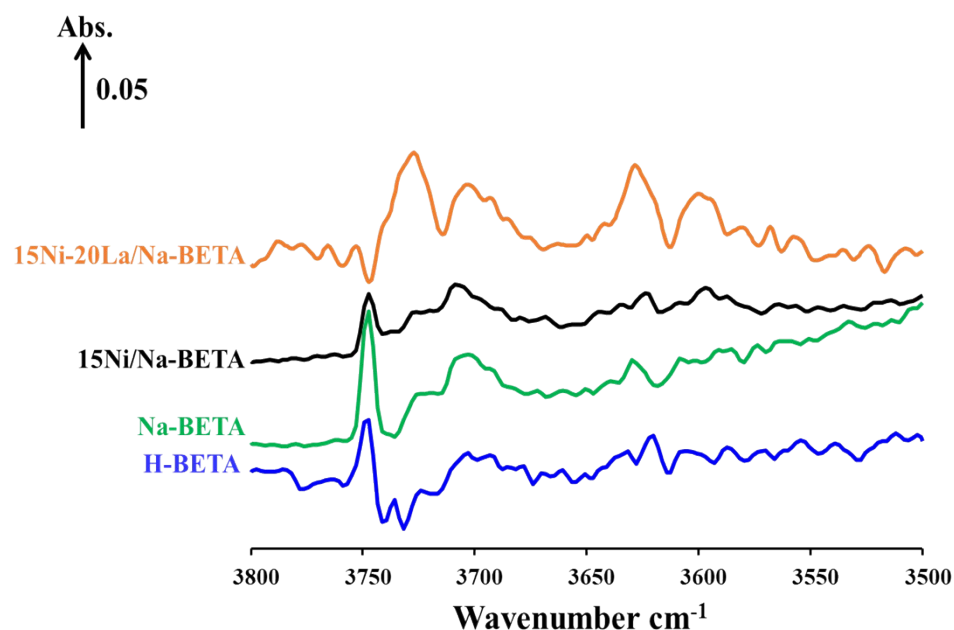

Fig. S12. Comparison of the IR spectra in the wavenumber range (3,500 -3,800 cm^{-1}) for different samples.

References

[1] A. Quindimil, U. De-La-Torre, B. Pereda-Ayo, J.A. González-Marcos, J.R. González-Velasco, Ni catalysts with La as promoter supported over Y- and BETA- zeolites for CO_2 methanation, Applied Catalysis B: Environmental, 238 (2018) 393-403.

[2] A.N. Pinheiro, A. Valentini, J.M. Sasaki, A.C. Oliveira, Highly stable dealuminated zeolite support for the production of hydrogen by dry reforming of methane, Applied Catalysis A: General, 355 (2009) 156-168.

[3] G. Naresh, V. Vijay Kumar, C. Anjaneyulu, J. Tardio, S.K. Bhargava, J. Patel, A. Venugopal, Nano size Hβ zeolite as an effective support for Ni and NiCu for CO_x free hydrogen production by catalytic decomposition of methane, International Journal of Hydrogen Energy, 41 (2016) 19855-19862.

[4] S. Abate, C. Mebrahtu, E. Giglio, F. Deorsola, S. Bensaid, S. Perathoner, R. Pirone, G. Centi, Catalytic Performance of γ-Al_2O_3–ZrO_2–TiO_2–CeO_2 Composite Oxide Supported Ni-Based Catalysts for CO2 Methanation, Industrial & Engineering Chemistry Research, 55 (2016) 4451-4460.

[5] Q. Liu, F. Gu, X. Lu, Y. Liu, H. Li, Z. Zhong, G. Xu, F. Su, Enhanced catalytic performances of Ni/Al_2O_3 catalyst via addition of V_2O_3 for CO methanation, Applied Catalysis A: General, 488 (2014) 37-47.

[6] B. Pawelec, R. Mariscal, R.M. Navarro, J.M. Campos-Martin, J.L.G. Fierro, Simultaneous 1-pentene hydroisomerisation and thiophene hydrodesulphurisation over sulphided Ni/FAU and Ni/ZSM-5 catalysts, Applied Catalysis A: General, 262 (2004) 155-166.

[7] I. Graça, L.V. González, M.C. Bacariza, A. Fernandes, C. Henriques, J.M. Lopes, M.F. Ribeiro, CO_2 hydrogenation into CH_4 on NiHNaUSY zeolites, Applied Catalysis B: Environmental, 147 (2014) 101-110.

[8] A. Śrębowata, R. Baran, D. Łomot, D. Lisovytskiy, T. Onfroy, S. Dzwigaj, Remarkable effect of postsynthesis preparation procedures on catalytic properties of Ni-loaded BEA zeolites in hydrodechlorination of 1,2-dichloroethane, Applied Catalysis B: Environmental, 147 (2014) 208-220.

[9] A. Śrębowata, I. Zielińska, R. Baran, G. Słowik, S. Dzwigaj, Ag–Ni bimetallic SiBEA zeolite as an efficient catalyst of hydrodechlorination of 1,2-dichloroethane towards ethylene, Catalysis Communications, 69 (2015) 154-160.

[10] P.M. Lima, T. Garetto, C.L. Cavalcante, D. Cardoso, Isomerization of n-hexane on Pt–Ni catalysts supported on nanocrystalline H-BEA zeolite, Catalysis Today, 172 (2011) 195-202.

[11] Z. Zheng, C. Sun, R. Dai, S. Wang, X. Wu, X. An, Z. Wu, X. Xie, Ethanol Steam Reforming on Ni-Based Catalysts: Effect of Cu and Fe Addition on the Catalytic Activity and Resistance to Deactivation, Energy & Fuels, 31 (2017) 3091-3100.

[12] J. Aguado, D.P. Serrano, J.M. Escola, L. Briones, Deactivation and regeneration of a Ni supported hierarchical Beta zeolite catalyst used in the hydroreforming of the oil produced by LDPE thermal cracking, Fuel, 109 (2013) 679-686.

[13] D.P. Serrano, J.M. Escola, L. Briones, S. Medina, A. Martínez, Hydroreforming of the oils from LDPE thermal cracking over Ni–Ru and Ru supported over hierarchical Beta zeolite, Fuel, 144 (2015) 287-294.

[14] C. Mebrahtu, S. Abate, S. Perathoner, S. Chen, G. Centi, CO_2 methanation over Ni catalysts based on ternary and quaternary mixed oxide: A comparison and analysis of the structure-activity relationships, Catalysis Today, 304 (2018) 181-189.

[15] S. Abate, K. Barbera, E. Giglio, F. Deorsola, S. Bensaid, S. Perathoner, R. Pirone, G. Centi, Synthesis, Characterization, and Activity Pattern of Ni–Al Hydrotalcite Catalysts in CO_2 Methanation, Industrial & Engineering Chemistry Research, 55 (2016) 8299-8308.

[16] Z. Boukha, L. Fitian, M. López-Haro, M. Mora, J.R. Ruiz, C. Jiménez-Sanchidrián, G. Blanco, J.J. Calvino, G.A. Cifredo, S. Trasobares, S. Bernal, Influence of the calcination temperature on the nano-structural properties, surface basicity, and catalytic behavior of alumina-supported lanthana samples, Journal of Catalysis, 272 (2010) 121-130.

[17] H.-W. Kim, K.-M. Kang, H.-Y. Kwak, J.H. Kim, Preparation of supported Ni catalysts on various metal oxides with core/shell structures and their tests for the steam reforming of methane, Chemical Engineering Journal, 168 (2011) 775-783.

[18] Alcalde-Santiago, V.; Davó-Quiñonero, A.; Lozano-Castelló, D.; Quindimil, A.; De-La-Torre, U.; Pereda-Ayo, B.; González-Marcos, J. A.; González-Velasco, J. R.; Bueno-López, A., Ni/LnO$_x$ Catalysts (Ln=La, Ce or Pr) for CO$_2$ Methanation. ChemCatChem 2019, 11 (2), 810-819.

[19] Huang, J.; Jiang, Y.; Reddy Marthala, V. R.; Ooi, Y. S.; Weitkamp, J.; Hunger, M., Concentration and acid strength of hydroxyl groups in zeolites La, Na-X and La, Na-Y with different lanthanum exchange degrees studied by solid-state NMR spectroscopy. Microporous and Mesoporous Materials 2007, 104 (1), 129-136.